2024 6th International Conference on Reconfigurable
Mechanisms and Robots (ReMAR)
June 24-27, 2024. Chicago, IL, USA

Output Mode Switching for Parallel Five-bar Manipulators Using a Projection-based Direct Collocation Method

Shashank Ramesh,[1] Patrick M. Wensing,[1] and Mark Plecnik[1]

2024 6th International Conference on Reconfigurable Mechanisms and Robots (ReMAR) | 979-8-3503-9596-9/24/$31.00 ©2024 IEEE | DOI: 10.1109/REMAR61031.2024.10617557

***Abstract*— For a given endpoint position, a five-bar manipulator may assume several separate configurations, with each offering distinct differential kinematics. The corresponding configurations are separated by output singularities and are said to belong to different output modes. In this work, a procedure for dynamically switching between output modes is proposed, with each mode offering different directional force/velocity transmission ratios. The procedure involves solving an optimal control problem using a projection-based direct collocation method for constrained mechanisms to find an optimal trajectory along which the mechanism changes output modes. Using this procedure, a five-bar mechanism configured at a given end-effector position is shown to switch to another output mode where the electrical energy consumed by the actuators to statically hold the mechanism reduces by 80%. Furthermore, the computed trajectories are seen to cross input singularities, a maneuver made possible by momentum planning since actuator authority is impaired at these configurations.**

I. Introduction

Both serial and parallel mechanisms can be assembled into multiple configurations given the coordinates of their end-effector, i.e., there are multiple inverse kinematic (IK) solutions. In particular, a five-bar mechanism generally has up to four real IK solutions. For example, two of the IK solutions of the five-bar mechanism considered in this work are shown in Fig. 1. Since these solutions correspond to different configurations of the five-bar mechanism, their local differential properties dictate different directional force/velocity transmission ratios. This implies that at the same end-effector position, different ranges of end-effector velocity and force can be produced by simply reconfiguring to different IK solutions. For example, the configuration in Fig. 1(a) can achieve high end-effector velocities along the y-axis for small actuator velocities, whereas the configuration in Fig. 1(b) can produce high end-effector forces along the y-axis for small actuator torques. Such switchable properties can be advantageous for mobile robots that hold their own weight with limbs. The neighborhood of configurations indicated in Fig. 1(b) can be energy efficient for standing, whereas the neighborhood of configurations indicated in Fig. 1(a) is suited for jumping. Thus, switching between the configurations in Fig. 1 can improve efficiency and jumping performance.

It is the case for the five-bar mechanism that moving between IK solutions involves crossing *output singularities*. Output singularities are the singular solutions to the inverse kinematics problem. They form curves in the five-bar's configuration space that when projected onto the Cartesian output space indicate workspace bounds (local or global). These curves partition the configuration space into separate regions, called *output modes*. For the case of the five-bar, IK solutions are necessarily separated by output singularities, although this is not generically true [1]. Each output mode can differ in terms of its transmission properties and bounding output singularities as shown in Fig. 1. Switching between output modes geared for different tasks forms the motivation for this work.

In literature, switching configurations of parallel robots by crossing singularities has been studied for workspace enlargement in [2]–[4]. Specifically for the five-bar mechanism, Macho et. al. in [5] describe crossing output singularities to access the desired portions of the workspace. A graph search method is proposed in [6] to switch between output modes of a five-bar mechanism. These methods consider only the kinematics of parallel robots and tend to be computationally expensive due to exhaustive sampling of the configuration space. In [7], minimum-time trajectories are planned to switch output modes considering the dynamics of the five-bar mechanism. In contrast, this work uses an optimal control strategy to plan a trajectory between configurations in different output modes with the objective of minimizing actuator torques. Optimal-control-based path planning for a five-bar mechanism is detailed in [8] where Pontryagin's minimum principle is used. By contrast, this paper contributes a method for designing trajectories capable of switching output modes based on a direct collocation approach that is compatible with closed-chain mechanisms [9]. This method enables singularity-free computations even at physical singularities of the mechanism and does not rely on exhaustive sampling of the configuration space, thereby speeding computations.

The rest of the paper is organized as follows. Section II presents the background concepts relevant to this work. The kinematics, dynamics, and optimal control problem for the five-bar mechanism are formulated and a solution method is proposed in Section III. Subsequently, Section IV presents two numerical examples of switching output modes for the five-bar in Fig. 1. Finally, the discussion of results and conclusion are presented in Sections V and VI, respectively.

II. Background

For a five-bar mechanism with input joint angles $\phi, \psi \in \mathbb{R}$, intermediate joint angles $\rho, \theta \in \mathbb{R}$ and output end-effector position $\boldsymbol{P} \in \mathbb{R}^2$, the kinematic constraints can be written

*This material is based upon work supported by the National Science Foundation under Grant No. CMMI-2144732.

[1]All authors are with Department of Aerospace and Mechanical Engineering, University of Notre Dame, Notre Dame, IN 46556 USA {sramesh,pwensing,plecnikmark}@nd.edu

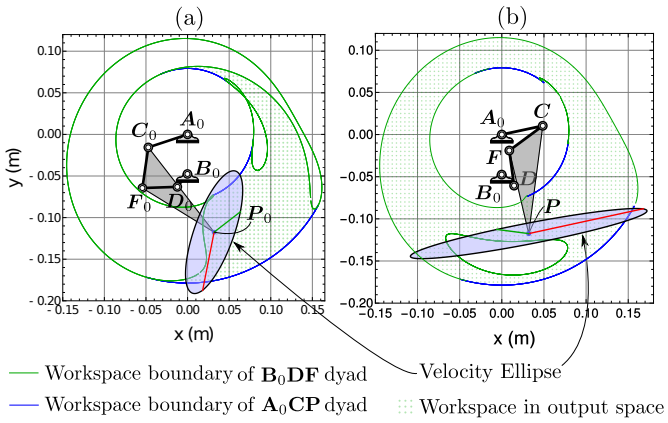

Fig. 1. Five-bar mechanism configured in two different output modes. The configuration in (a) can achieve high end-effector velocities in the vertical direction compared to the configuration in (b) which makes it suitable for jumping. The configuration in (b) can support high vertical forces compared to the one in (a) and is suited for standing while consuming low energy.

as:

$$[\boldsymbol{\eta}(\phi,\psi,\rho,\theta) \;\; \boldsymbol{\zeta}(\phi,\rho,\boldsymbol{P})]^\top = \mathbf{0} \in \mathbb{R}^4 \tag{1}$$

Angles ρ, θ can be eliminated to obtain $\boldsymbol{g}(\boldsymbol{\theta}, \boldsymbol{P}) = \mathbf{0} \in \mathbb{R}^2$, where $\boldsymbol{\theta} = [\phi \;\; \psi]^\top$. Further details on these constraints are presented in Section III-A. From the total derivative of $\boldsymbol{g}$, we get the relation between the input and output velocities:

$$\dot{\boldsymbol{P}} = [J]\dot{\boldsymbol{\theta}}, \quad \text{where} \tag{2}$$
$$[J] = -\left[\frac{\partial \boldsymbol{g}}{\partial \boldsymbol{P}}\right]^{-1}\left[\frac{\partial \boldsymbol{g}}{\partial \boldsymbol{\theta}}\right] \quad \text{assuming} \quad \left|\frac{\partial \boldsymbol{g}}{\partial \boldsymbol{P}}\right| \neq 0.$$

In Eq. (2), matrix $[J]$ is known as the Jacobian matrix. This Jacobian matrix maps a unit circle in the input velocity space to a *velocity ellipse* (or manipulability ellipse) in the output velocity space as detailed in [10, pp. 148]. Figure 1(a) shows the velocity ellipse at the end-effector for a particular configuration of the five-bar mechanism considered in this work. Along the minor axis of the velocity ellipse, the end-effector force production is maximum. Hence, the configuration in Fig. 1(b) can support relatively high vertical forces at the end-effector with low actuator torques and is, therefore, suited for standing while consuming low energy. Further, since the major axis of the velocity ellipse in Fig. 1(a) is nearly vertical, the end-effector can move at high velocities in the vertical direction which is useful for jumping.

When $\left|\frac{\partial \boldsymbol{g}}{\partial \boldsymbol{\theta}}\right| = 0$, then the minor axis length of the velocity ellipse goes to zero and the mechanism is at a workspace boundary or an *output singularity*. At an output singularity, there exist actuator velocities that instantaneously produce zero end-effector velocity in the direction normal to the workspace bound. If $\left|\frac{\partial \boldsymbol{g}}{\partial \boldsymbol{P}}\right| = 0$, the major axis length of the velocity ellipse goes to infinity and the mechanism is at an *input singularity*. Input singularities are boundaries in the input space, i.e., the space of the two actuator angles. At an input singularity, there instantaneously exists a direction in the output space in which force transmission from the actuators maps to zero at the end-effector.

The set of all configurations of the five-bar mechanism defines the configuration space of the mechanism. The input singularities divide the configuration space into several regions known as input modes. Similarly, the regions separated by output singularities are known as output modes. The projection of the subset of output singularities that bound a given output mode onto the output space gives the workspace boundary of that output mode in the output space. Hence, the workspace boundaries are different for different output modes. For example, the configurations in Fig. 1 are in different output modes and have different workspace boundaries. In this work, two examples are considered where the configurations belong to different input and/or output modes.

In order to plan a path between two configurations in different output modes, an optimal control approach using the direct collocation method is followed in this work. Consider an optimization problem of the form:

$$\min_u \frac{1}{2}\int_0^T \boldsymbol{x}(t)^\top [Q]\, \boldsymbol{x}(t) + \boldsymbol{u}(t)^\top [R]\, \boldsymbol{u}(t), \tag{3}$$
$$\dot{\boldsymbol{x}}(t) = \boldsymbol{f}(\boldsymbol{x}(t), \boldsymbol{u}(t)) \in \mathbb{R}^n, \tag{4}$$

where $\boldsymbol{x} \in \mathbb{R}^n, \boldsymbol{u} \in \mathbb{R}^m$; the weight matrices are $[Q] \in \mathbb{R}^{n\times n}, [R] \in \mathbb{R}^{m\times m}$; $t \in \mathbb{R}$ is a parameter and T is a given constant. For robot mechanisms, Eq. (4) would define the robot dynamics with $\boldsymbol{x}$ as the states (configuration and velocities) of the robot, $\boldsymbol{u}$ as inputs (actuator torques) to the robot and t as time. In direct collocation, t is discretized into N finite elements and N_c collocation points within each finite element. The states at the collocation points need to follow collocation constraints that approximate the ODE in Eq. (4). In this work, the Gauss-Radau collocation scheme is used to choose collocation points [11]. A polynomial of degree N_c that interpolates the collocation points represents an approximate solution to Eq. (4) in each finite element. The interpolating polynomial also gives a quadrature rule to approximate $\boldsymbol{x}$ at the end of each finite element. Using this method, the dynamic equations of a robot mechanism can be discretized and imposed as algebraic constraints in the optimal control problem. The mathematical details of this method are presented in Section III.

It is worth noting that only dynamic equations describing a robot's model were considered in the direct collocation method discussed above. However, for constrained mechanisms like the five-bar considered in this work, even though the dynamics are defined to satisfy the kinematic constraints locally, taking discrete steps according to direct collocation leads to constraint violation as seen in Fig. 2. Therefore,

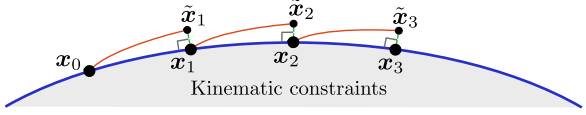

Fig. 2. Qualitative depiction of the solution obtained for the projection based direct collocation method presented in [9]. The initial state is given by $\boldsymbol{x}_0$. The states obtained from the quadrature rule are $\tilde{\boldsymbol{x}}_1, \tilde{\boldsymbol{x}}_2, \tilde{\boldsymbol{x}}_3$ and their projections onto the kinematic constraints are given by $\boldsymbol{x}_1, \boldsymbol{x}_2, \boldsymbol{x}_3$.

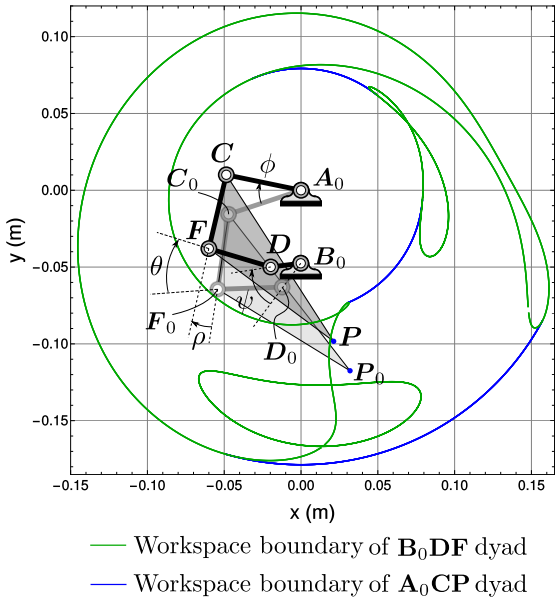

Fig. 3. Kinematic diagram of the five-bar mechanism displaced from a reference configuration.

kinematic constraints also need to be considered to ensure that the discretized states in direct collocation also satisfy the kinematic constraints. However, simply imposing kinematic constraints as additional constraints in direct collocation leads to an over-constrained problem since the discretized states are already well-defined by the collocation constraints and quadrature rules. Another method would be to parameterize the states of the five-bar in terms of some global minimal coordinates which eliminates the kinematic constraints. However, this formulation is not free of singularities for many robot systems including the five-bar mechanism considered in this work. Hence, following the projection-based direct collocation method in [9], new optimization variables, namely $\tilde{\boldsymbol{x}}_k, k = 1, 2, \ldots, N$, are introduced for the states obtained from quadrature rule and are projected onto the constraint manifold to get $\boldsymbol{x}_k$ as depicted in Fig. 2. This method is discussed in more detail for the problem considered in this work in the subsequent section.

III. Problem Formulation

Given the initial and final configurations of the five-bar mechanism that are in different output modes, the task is to plan a trajectory between the two configurations. For this, the kinematics, dynamics, and optimal control problem are formulated and a solution procedure is detailed in this section.

A. Kinematics and Dynamics

Figure 3 shows the kinematic diagram of the five-bar mechanism displaced from a known reference configuration given by: $\boldsymbol{A}_0, \boldsymbol{B}_0, \boldsymbol{C}_0, \boldsymbol{D}_0, \boldsymbol{F}_0, \boldsymbol{P}_0$. The actuators situated at $\boldsymbol{A}_0$ and $\boldsymbol{B}_0$ are fixed to ground and displace the links $\boldsymbol{A}_0\boldsymbol{C}$ and $\boldsymbol{B}_0\boldsymbol{D}$ by angles[1] ϕ and ψ, respectively. The kinematic constraints in Eq. (1) are given by:

$$\begin{aligned}\boldsymbol{\eta} &= \boldsymbol{A}_0 + [\mathcal{R}(\phi)]\,(\boldsymbol{C}_0 - \boldsymbol{A}_0) + [\mathcal{R}(\rho)]\,(\boldsymbol{F}_0 - \boldsymbol{C}_0) \\ &\quad - \boldsymbol{B}_0 + [\mathcal{R}(\psi)]\,(\boldsymbol{D}_0 - \boldsymbol{B}_0) + [\mathcal{R}(\theta)]\,(\boldsymbol{F}_0 - \boldsymbol{D}_0) = \boldsymbol{0}, \quad (5)\\ \boldsymbol{\zeta} &= \boldsymbol{A}_0 + [\mathcal{R}(\phi)]\,(\boldsymbol{C}_0 - \boldsymbol{A}_0) + [\mathcal{R}(\rho)]\,(\boldsymbol{P}_0 - \boldsymbol{C}_0) - \boldsymbol{P} = \boldsymbol{0}. \quad (6)\end{aligned}$$

In Eqs. (5, 6), ρ and θ describe the orientation of the passive links $\boldsymbol{CF}$ and $\boldsymbol{DF}$, respectively. Differentiating Eqs. (5, 6) and eliminating $\dot{\rho}, \dot{\theta}$ gives $[J]$ in Eq. (2). If $[J]$ goes singular, then the mechanism is at an output singularity as described in Section II. At an output singularity, the links of either or both $\boldsymbol{A}_0\boldsymbol{CP}$ and $\boldsymbol{B}_0\boldsymbol{DF}$ dyads align. These output singularities in the output space, i.e., workspace boundaries, are shown in Fig. 3. However, note that for a given output mode, only portions of these workspace boundaries bound the output mode as explained in Section II. At input singularities, the joints $\boldsymbol{C}, \boldsymbol{F}, \boldsymbol{D}$ are collinear and $[J]$ does not exist since the inverse of $\left[\frac{\partial \boldsymbol{g}}{\partial \boldsymbol{P}}\right]$ does not exist.

The configuration of the mechanism is defined uniquely by $\boldsymbol{q} = [\phi\ \psi\ \rho\ \theta]^\top$. The set of all $\boldsymbol{q}$ that satisfy Eq. (5) forms the configuration space of the five-bar mechanism. The dynamics of the five-bar mechanism is formulated using the *Lagrangian equation of motion* given by:

$$[M(\boldsymbol{q})]\,\ddot{\boldsymbol{q}} + [C_m(\boldsymbol{q}, \dot{\boldsymbol{q}})]\,\dot{\boldsymbol{q}} + \boldsymbol{G}(\boldsymbol{q}) = [J_{\eta q}]^\top \boldsymbol{\lambda}_f + \boldsymbol{Q}_{nc}. \quad (7)$$

In Eq. (7), $[M(\boldsymbol{q})] \in \mathbb{R}^{4\times4}$ is the mass matrix, $[C_m(\boldsymbol{q}, \dot{\boldsymbol{q}})] \in \mathbb{R}^{4\times4}$ is a Coriolis matrix [12], $\boldsymbol{G}(\boldsymbol{q}) \in \mathbb{R}^4$ is the gravity vector, $[J_{\eta q}] = \left[\frac{\partial \boldsymbol{\eta}}{\partial \boldsymbol{q}}\right]$ is the Jacobian matrix of the constraints, $[J_{\eta q}]^\top \boldsymbol{\lambda}_f$ is the vector of generalized constraint forces and $\boldsymbol{Q}_{nc} = [\tau_1\ \tau_2\ 0\ 0]^\top$, where τ_1 and τ_2 are the actuator torques at joints $\boldsymbol{A}_0$ and $\boldsymbol{B}_0$, respectively. Gravity is assumed to act downwards along the negative y-axis in the reference frame in Fig. 3. The ODEs in Eq. (7) along with the constraints $\boldsymbol{\eta} = 0$ in Eq. (5) form a set of differential algebraic equations (DAE) that defines the dynamic model of the mechanism. Alternatively, the unknowns $\boldsymbol{\lambda}_f \in \mathbb{R}^2$ can be eliminated from the DAE using the double derivative of $\boldsymbol{\eta} = \boldsymbol{0}$ to get:

$$\begin{aligned}\dot{\boldsymbol{x}} &= \begin{bmatrix} \dot{\boldsymbol{q}} \\ [M]^{-1}\,(\boldsymbol{h}_1 - [J_{\eta q}]^\top\,[A_m]^{-1}\,\boldsymbol{h}_2) \end{bmatrix} \quad (8)\\ &= \boldsymbol{f}(\boldsymbol{x}, \boldsymbol{\tau}), \quad \text{where} \quad (9)\\ [A_m] &= [J_{\eta q}]\,[M]^{-1}\,[J_{\eta q}]^\top \\ \boldsymbol{h}_1 &= \boldsymbol{Q}_{nc} - [C_m]\,\dot{\boldsymbol{q}} - \boldsymbol{G}, \\ \boldsymbol{h}_2 &= ([\dot{J}_{\eta q}]\dot{\boldsymbol{q}} + [J_{\eta q}]\,[M]^{-1}\,\boldsymbol{h}_1), \\ \boldsymbol{x} &= [\boldsymbol{q}\ \dot{\boldsymbol{q}}]^\top.\end{aligned}$$

Given the actuator torques $\boldsymbol{\tau} = [\tau_1\ \tau_2]^\top$, solving the ODE in Eq. (8) yields states $\boldsymbol{x}$ that satisfy the following kinematic constraints:

$$\boldsymbol{f}_c(\boldsymbol{x}) = [\ \boldsymbol{\eta}(\boldsymbol{q})\quad [J_{\eta q}(\boldsymbol{q})]\,\dot{\boldsymbol{q}}\ ]^\top = \boldsymbol{0}. \quad (10)$$

[1]All angles in this manuscript are measured in radians until otherwise mentioned explicitly.

With this dynamic model, an optimal control problem is formulated in the next section.

B. Optimal Control Problem

The goal is to reach a given final configuration $\boldsymbol{q}_F$ starting from a known initial configuration $\boldsymbol{q}_I$ in a given time T. If E_I and E_F are the total energies (kinetic and potential energy) of the mechanism at $\boldsymbol{q}_I$ and $\boldsymbol{q}_F$, respectively, the net mechanical work done in moving from $\boldsymbol{q}_I$ to $\boldsymbol{q}_F$ is $W_{IF} = E_F - E_I$. Since W_{IF} does not depend on the trajectory followed to move from $\boldsymbol{q}_I$ to $\boldsymbol{q}_F$, the portion of electrical energy consumed by the actuators to do this work is fixed for the given $\boldsymbol{q}_I$ and $\boldsymbol{q}_F$. However, the rest of the electrical energy consumed by the actuators is dissipated as Joule heating which depends on the trajectory between $\boldsymbol{q}_I$ and $\boldsymbol{q}_F$. Assuming identical BLDC actuators with torque constant K_t and winding resistance R_w, the electrical power dissipated as Joule heat is:

$$P_t = \frac{R}{K_t^2}\boldsymbol{\tau}^\top\boldsymbol{\tau}. \tag{11}$$

With the objective of minimizing the total energy dissipated as Joule heat to reach $\boldsymbol{q}_F$ starting from $\boldsymbol{q}_I$, the following optimal control problem is formulated:

$$\min_{\boldsymbol{\tau}} \frac{R}{K_t^2}\int_0^T \boldsymbol{\tau}^\top\boldsymbol{\tau}\ \mathrm{d}t \tag{12}$$

$$\text{s.t.}\quad \dot{\boldsymbol{x}} = \boldsymbol{f}(\boldsymbol{x},\boldsymbol{\tau}). \tag{13}$$

The above optimal control problem is of the same form as Eqs. (3, 4) with[2] $[Q] = [\,0\,]_{2\times2}$, $[R] = 2(R/K_t^2)[\,I\,]_{2\times2}$, $\boldsymbol{u} = \boldsymbol{\tau}$ which is solved using the direct collocation method. According to this method, the time domain is discretized uniformly into N time steps, i.e., $t_k \in [0\ T], k = 1, 2, \ldots, N$ with a time interval of $h = T/N$. Let N_c be the number of collocation points in each time interval $[t_k\ \ t_{k+1}]$ that are chosen according to the Gauss-Radau collocation scheme. The states, actuator torques, and time at each collocation point are denoted by $\boldsymbol{x}_{kj}, \boldsymbol{\tau}_{kj}$ and t_{kj}, respectively, for $k = 1, 2, \ldots, N$ and $j = 1, 2, \ldots, N_c$. The optimization problem can now be written as

$$\min_{\boldsymbol{\tau}} \sum_{k=1}^{N} h\sum_{j=1}^{N_c} w_j\boldsymbol{\tau}_{kj}^\top\boldsymbol{\tau}_{kj} \tag{14}$$

$$\text{s.t.}\quad \dot{\boldsymbol{x}}_{kj} = \boldsymbol{f}(\boldsymbol{x}_{kj},\boldsymbol{\tau}_{kj}), \tag{15}$$

$$\boldsymbol{x}_{kj} = \boldsymbol{x}_k + h\sum_{i=1}^{N_c}\beta_{ji}\dot{\boldsymbol{x}}_{ki}, \tag{16}$$

$$\boldsymbol{x}_{k+1} = \boldsymbol{x}_k + h\sum_{j=1}^{N_c} w_j\dot{\boldsymbol{x}}_{kj}, \tag{17}$$

where w_j, β_{ji} are the weights computed according to the Gauss-Radau collocation scheme [11]. Equations (15, 16) define the collocation constraints and Eq. (17) is the quadrature rule. Since the direct collocation method approximates the ODE in Eq. (8) through discretization, the optimal trajectory obtained by solving Eqs. (14-17) may not satisfy the kinematic constraints in Eq. (10) as discussed in Section II. To account for the kinematic constraints, the projection-based direct collocation method presented in [9] is followed. Let $\tilde{\boldsymbol{x}}_{k+1}$ denote the state at the end of the interpolating polynomial between t_k and t_{k+1} time interval. This state does not necessarily satisfy the kinematic constraints and is computed according to the quadrature rule:

$$\tilde{\boldsymbol{x}}_{k+1} = \boldsymbol{x}_k + h\sum_{j=1}^{N_c} w_j\dot{\boldsymbol{x}}_{kj}. \tag{18}$$

In Eq. (18), $\boldsymbol{x}_k$ denotes the state at t_k that satisfies the kinematic constraints. To compute $\boldsymbol{x}_{k+1}$ that satisfies the kinematic constraints, new variables $\boldsymbol{\mu}_{k+1} \in \mathbb{R}^4$ are introduced and $\tilde{\boldsymbol{x}}_{k+1}$ is projected onto the constraint manifold in Eq. (10) as:

$$\boldsymbol{x}_{k+1} = \tilde{\boldsymbol{x}}_{k+1} + \left[\,\frac{\partial \boldsymbol{f}_c}{\partial \boldsymbol{x}}\,\right]\Bigg|^{\top}_{\boldsymbol{x}=\boldsymbol{x}_{k+1}} \boldsymbol{\mu}_{k+1}, \tag{19}$$

$$\boldsymbol{f}_c(\boldsymbol{x}_{k+1}) = \boldsymbol{0}. \tag{20}$$

In Eq. (19), $\boldsymbol{\mu}_{k+1}$ is the vector of Lagrange multipliers associated with the projection of $\tilde{\boldsymbol{x}}_{k+1}$ onto the constraint manifold. Thus, the optimization problem is reformulated by replacing Eq. (17) with Eqs. (18-20). The states at the collocation points can also be projected onto the constraint manifold as explained in [9]. However, this introduces additional variables in the optimization problem. Since the constraint drift within each element was observed to be low, only the state at the end of each element was projected thereby leading to a simpler optimization problem with fewer optimization variables.

The optimization problem is set up in Python using the `CasADi` package [13] and solved using the `IPOPT` method [14]. Since a local optimization method is chosen, a good initial guess for the trajectory is crucial for obtaining feasible solutions. Depending on the input modes that the initial and final configurations belong to, two heuristic methods are proposed for finding an initial guess trajectory. **Case I** *where $\boldsymbol{q}_I$ and $\boldsymbol{q}_F$ belong to the same input mode*: A family of circular arcs joining $\boldsymbol{\theta}_I = [\phi_I, \psi_I]^\top$ and $\boldsymbol{\theta}_F = [\phi_F, \psi_F]^\top$ were considered. The shape of the arcs was parameterized by curvature α, and their traversal was parameterized by arc length s: $\boldsymbol{\theta}(s,\alpha) = \boldsymbol{\Phi}_{IF}(s,\alpha), s \in [0,1]$ such that $\boldsymbol{\theta}(0,\alpha) = \boldsymbol{\theta}_I$ and $\boldsymbol{\theta}(1,\alpha) = \boldsymbol{\theta}_F$. For a set of curvatures α_i, configurations $\boldsymbol{q}_i(s)$ were computed along the path $\boldsymbol{\theta}(s,\alpha_i)$ using forward kinematics.[3] Assuming a trapezoidal velocity profile for $s(t)$, the trajectories $\boldsymbol{q}_i(t), \dot{\boldsymbol{q}}_i(t), \ddot{\boldsymbol{q}}_i(t)$ were computed. The velocity and acceleration parameters for the trapezoidal velocity profile were chosen based on the path length and the time needed to traverse the path. Subsequently, the torques $\boldsymbol{\tau}_i(t)$ required to realize $\boldsymbol{q}_i(t), \dot{\boldsymbol{q}}_i(t), \ddot{\boldsymbol{q}}_i(t)$ were computed from Eq. (8).

[2]In this manuscript, $[\,0\,]_{2\times2}$ and $[\,I\,]_{2\times2}$ denote the 2×2 zero matrix and identity matrix, respectively.

[3]Note that the forward kinematic solutions are unique since the input mode is known

Evaluating the sum of square of torques, i.e., the objective in Eq. (14), for each i, the trajectory with the least objective value was chosen as the initial guess trajectory for the optimization problem.

Case II *where $\boldsymbol{q}_I$ and $\boldsymbol{q}_F$ do not belong to the same input mode*: In this case, the trajectory joining $\boldsymbol{q}_I$ and $\boldsymbol{q}_F$ has to cross input singularities to switch input modes. The method in Case I cannot be applied since the trajectories do not cross input singularities. The initial guess trajectory in this case was simply assumed to be a linear interpolation between $\boldsymbol{q}_I$ and $\boldsymbol{q}_F$ with zero velocities and actuator torques. Note that this initial guess will not satisfy the kinematic and dynamic constraints as in Case I.

The resulting optimal states and torques are denoted as $\boldsymbol{x}_k^* = [\boldsymbol{q}_k^* \;\; \dot{\boldsymbol{q}}_k^*]^\top$ and $\boldsymbol{\tau}_k^*$, respectively. The kinematic and dynamic feasibility of optimal trajectories were verified by evaluating the following error metrics:

Kinematic constraint residual: The states along the optimal trajectory are substituted into the kinematic constraints in Eq. (10) to get $r_{p_k} = \|\boldsymbol{\eta}(\boldsymbol{q}_k^*)\|, r_{v_k} = \|\,[J_{\eta q}(\boldsymbol{q}_k^*)]\,\dot{\boldsymbol{q}}_k^*\|$. The position and velocity error metrics are defined as $r_p = \frac{1}{N}\sqrt{\sum_{k=0}^{N} r_{p_k}^2}$ and $r_v = \frac{1}{N}\sqrt{\sum_{k=0}^{N} r_{v_k}^2}$, respectively.

Energy conservation residual: The change in total energy at each state along the optimal trajectory, given by $\frac{\mathrm{d}E}{\mathrm{d}t}(\boldsymbol{x}_k^*)$, must be equal to the instantaneous mechanical power $P_k = [\dot{\phi}_k^* \;\; \dot{\psi}_k^*]\cdot\boldsymbol{\tau}_k^*$. This motivates the error metric $e = \frac{1}{N}\sqrt{\sum_{k=0}^{N} e_k^2}$, where $e_k = \frac{\mathrm{d}E}{\mathrm{d}t}(\boldsymbol{x}_k^*) - P_k$.

A computed trajectory is deemed acceptable if $r_p \leq 10^{-9}$ m, $r_v \leq 10^{-9}$ m/s and $e \leq 10^{-4}$ W. Computations were performed with double precision. The small dimensional and inertial parameters of the five-bar studied in this paper led to numerical scaling that hindered precision.

C. Metrics to Evaluate the Optimal Trajectory

For the optimal trajectory, two metrics were considered: (1) total electrical energy loss due to Joule heating (or thermal energy loss) in Eq. (14), and (2) root mean square (RMS) of torque exerted by each actuator along the trajectory, i.e., $\tau_i^{\mathrm{RMS}} = \frac{1}{N}\sqrt{\sum_{k=0}^{N} \tau_{i_k}^{*2}}, i = 1, 2$. Additionally, the sensitivity of each metric was quantified as described below.

In practice, the actuator torques may slightly deviate from $\boldsymbol{\tau}_k^*$ due to disturbance, denoted by $\boldsymbol{\tau}_{d_k}$. To study the effect of this on thermal energy loss, a feedforward PI controller was implemented for the actuators. Under this control law, if the actuator states at time t_k are ϕ_k, ψ_k, then the actuator torques $\boldsymbol{\tau}_k$ required to follow the desired trajectory ϕ_k^*, ψ_k^* are:

$$\boldsymbol{\tau}_k = \boldsymbol{\tau}_k^* + \boldsymbol{\tau}_{d_k} + [K_P]\,\boldsymbol{e}_k + [K_I]\sum_{j=1}^{k}\boldsymbol{e}_j, \quad \text{where,} \quad (21)$$

$$\boldsymbol{e}_k = [\phi_k^* - \phi_k \;\; \psi_k^* - \psi_k]^\top, \quad [K_P], [K_I] \in \mathbb{R}^{2\times 2}.$$

In Eq. (21), $[K_P]$ and $[K_I]$ are the proportional and integral gains, respectively, which are diagonal matrices. In this work, the gains are assumed to be $[K_P] = [\,I\,]_{2\times 2}$ Nm/rad, $[K_I] = 0.1[\,I\,]_{2\times 2}$ Nm/rad. Further, four possible torque disturbances are assumed that are constant for all time with magnitude of 3% of RMS torque given by $\boldsymbol{\tau}_{d_k} = \frac{3}{100}[\pm\tau_1^{\mathrm{RMS}} \;\; \pm\tau_2^{\mathrm{RMS}}]^\top$. The following simulation of the controller in Eq. (21) is carried out for each possible $\boldsymbol{\tau}_{d_k}$. At each step t_k, the torques are computed from the control law in Eq. (21) and are used to compute the states $\boldsymbol{x}_{k+1}$ at the next time step by solving Eq. (8). For $k > N$, the desired actuator states are $\phi_k^* = \phi_N^*$, $\psi_k^* = \psi_N^*$ and the torques $\boldsymbol{\tau}_k^*$ are computed from Eq. (8) with $\boldsymbol{x} = \boldsymbol{x}_N$ and $\dot{\boldsymbol{x}} = \boldsymbol{0}$. This simulation is carried out until ϕ_k and ψ_k lie within 1° of ϕ_N^* and ψ_N^*, respectively. The time taken for both ϕ_k and ψ_k to reach and stay within $\pm 1.5^\circ$ about ϕ_N^* and ψ_N^* is defined as the settling time and is denoted by T_{ss}. Subsequently, at each t_k, the total thermal energy loss starting from time t_0 is computed as $E_k = (R/K_t^2)\sum_{j=0}^{k} h\boldsymbol{\tau}_j^\top\boldsymbol{\tau}_j$. The thermal loss at T_{ss} is computed for each possible $\boldsymbol{\tau}_{d_k}$ and the highest value is compared with the optimal value obtained from Eq. (14).

In the subsequent section, two numerical examples are presented to demonstrate the procedure for switching output modes detailed in this section.

TABLE I

JOINT COORDINATES OF THE FIVE-BAR MECHANISM AT THE REFERENCE CONFIGURATION

	$\boldsymbol{B}_0$	$\boldsymbol{C}_0$	$\boldsymbol{D}_0$	$\boldsymbol{F}_0$	$\boldsymbol{P}_0$
x (mm)	0	−4.71	−1.23	−5.43	3.19
y (mm)	−4.75	−1.56	−6.31	−6.45	−11.75

IV. EXAMPLES

In this section, two numerical examples are considered to demonstrate output mode switching for the five-bar mechanism in Fig. 3. The dimensions of the five-bar are given in Table I in terms of the joint coordinates in the reference configuration. Note that $\boldsymbol{A}_0$ is fixed to the origin of the reference frame as shown in Fig. 3. The links $\boldsymbol{A}_0\boldsymbol{C}, \boldsymbol{FD}$, and $\boldsymbol{DB}_0$ are assumed to be cylindrical with diameter 6 mm and uniform density[4] 8000 kg/m^3. The masses of $\boldsymbol{CFP}$ link and the payload at the end-effector are assumed to be 0.2 kg and 0.5 kg, respectively. The moment of inertia of all links is assumed to be 0.01 kg m^2. The constant $R/K_t^2 = 1$ in Eq. (11). For both the examples, the initial configuration is $\boldsymbol{q}_I = [0\;0\;0\;0]^\top$ (see Fig. 1(a)), and the parameters in the optimization problem are chosen to be $T = 1.5$ s, $N = 100$ and $N_c = 4$.

A. Example 1

In this example, the five-bar needs to reach the configuration in Fig. 1(b) given by:

$$\boldsymbol{q}_F = [-3.250 \;\; 1.509 \;\; -0.789 \;\; -1.468]^\top. \quad (22)$$

The net mechanical work to be done to reach $\boldsymbol{q}_F$ is $W_{IF} = 0.062$ J. At $\boldsymbol{q}_I$ and $\boldsymbol{q}_F$, the actuator torques, namely $\boldsymbol{\tau}_I$

[4]All of the links of the five-bar are assumed to have uniform mass distribution, i.e., the center of mass lies at the centroid of the link

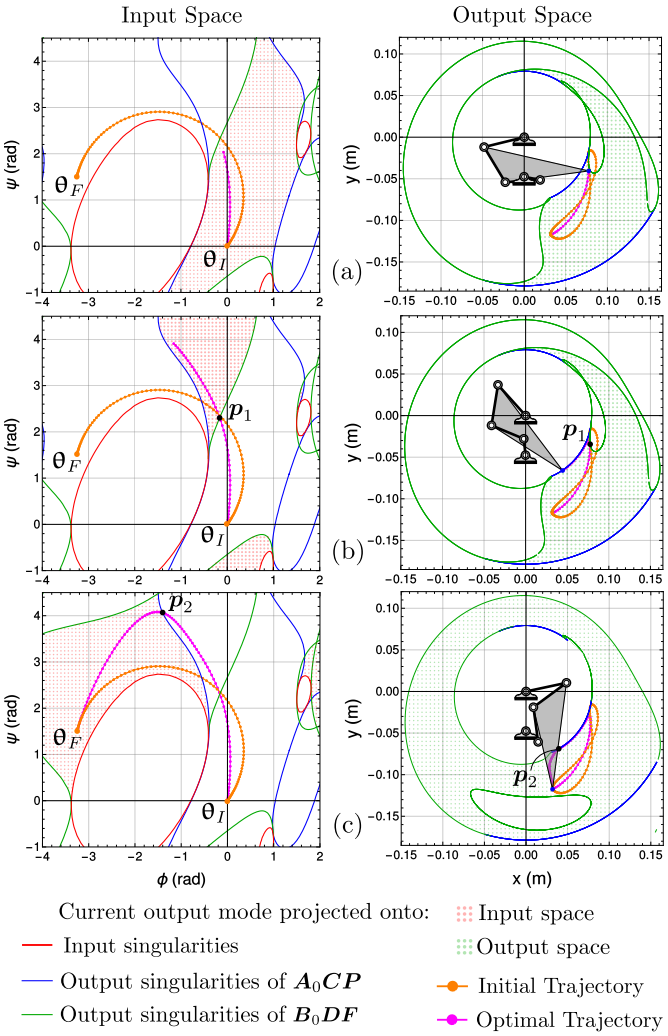

Fig. 4. Example 1: Configurations of the five-bar mechanism at time instants (a) $t = 0.36$ s, (b) $t = 0.735$ s, (c) $t = 1.5$ s, along the optimal trajectory. At each of these time instances, the regions in the input and output space accessible by the corresponding output mode are shaded. The initial guess trajectory and the optimal trajectory are shown in the actuator (input) space and the Cartesian (output) space.

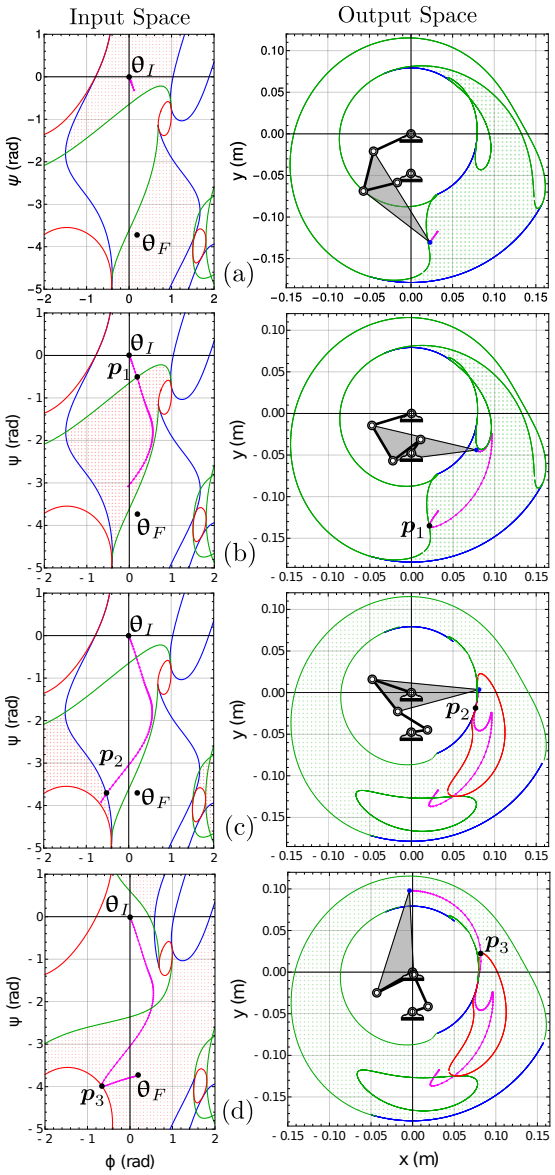

Fig. 5. Example 2: Configurations of the five-bar mechanism at time instants (a) $t = 0.135$ s, (b) $t = 0.885$ s, (c) $t = 1.035$ s, (d) $t = 1.5$ s, along the optimal trajectory. This figure shares a legend with Fig. 4.

and $\boldsymbol{\tau}_F$, respectively, needed to statically hold the mechanism is found from Eq. (8) by substituting $\dot{\boldsymbol{x}} = \mathbf{0}$ as:

$$\boldsymbol{\tau}_I = [-0.47 \quad 0.13\,]\ \text{Nm}, \quad \boldsymbol{\tau}_F = [\,0.21 \quad 0.04\,]\ \text{Nm}. \quad (23)$$

From Eq. (11), the electrical power dissipated as Joule heat for $\boldsymbol{\tau}_F$ is lower than that for $\boldsymbol{\tau}_I$ by 80%. This motivates switching output modes to configure in $\boldsymbol{q}_F$ instead of $\boldsymbol{q}_I$ for the same end-effector position.

Following the method for finding the initial guess trajectory explained in Section III, the circular trajectory in the input space in Fig. 4 is obtained. This trajectory is also shown in the output space of the manipulator in Fig. 4. With this initial trajectory, the optimal control problem was solved following the method in Section III and the resulting optimal trajectory and configurations are shown in Fig. 4 at different time instants. Along the optimal trajectory, the five-bar mechanism changes output mode for the first time at $\boldsymbol{p}_1$, where the links of $\boldsymbol{B_0DF}$ dyad align, after which the workspace in the input space changes as shown in Fig. 4(b). Subsequently, the output mode changes at $\boldsymbol{p}_2$, where the links of $\boldsymbol{A_0CP}$ dyad align, after which the workspace in the input and output space changes as seen in Fig. 4(c).

The electrical energy lost as Joule heat for initial and optimal trajectories were 0.621 J and 0.413 J which are $10\times$ and $6.6\times$ the minimum required work, respectively. The error metrics defined in Section III-C are found to be $r_p = 5.57\times10^{-11}$ m, $r_v = 7.82\times10^{-11}$ m/s and $e = 2.33\times10^{-6}$ W which are less than the tolerances stated in Section III-C. For the actuator at $\boldsymbol{A}_0$, the RMS torque for the initial and optimal trajectory is 0.578 Nm and 0.386 Nm, respectively. Similarly, the RMS torque for the actuator at $\boldsymbol{B}_0$ for the initial and optimal trajectory is 0.275 Nm and 0.354 Nm,

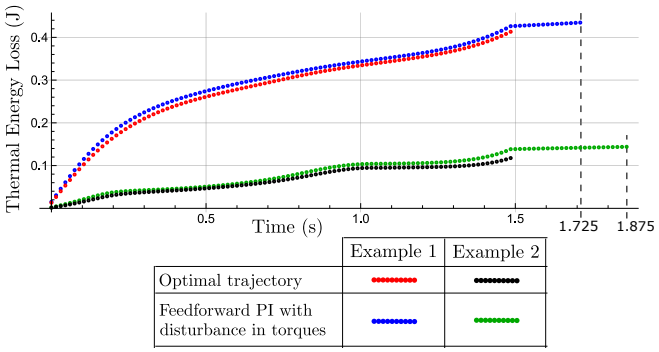

Fig. 6. Thermal energy loss over time along the optimal trajectory and for feedforward PI control with disturbance in actuator torques until the settling time T_{ss}.

respectively. Following the sensitivity analysis in Section III-C, the thermal energy loss was found to be maximum for positive disturbances. For this case, the thermal energy loss E_k is plotted with time and compared with the thermal energy loss along the optimal trajectory as shown in Fig. 6. For feedforward PI control with disturbance in torques as defined in Section III-C, the total thermal energy loss until $T_{ss} = 1.725$ s is 0.434 J which is 0.021 J higher than that for the optimal trajectory.

B. Example 2

In this example, the five-bar mechanism is desired to reach:

$$\boldsymbol{q}_F = [0.204 \;\; -3.733 \;\; 2.172 \;\; -1.181]^\top. \tag{24}$$

The motivation of this example is to reach a point in the output space which is not part of the initial output mode. The initial and final configurations are shown in Fig. 1(a) and Fig. 5(d), respectively. The work to be done to reach $\boldsymbol{q}_F$ is $W_{IF} = 1.24$ J. In this case, $\boldsymbol{q}_I$ and $\boldsymbol{q}_F$ belong to different input modes and hence, the method in Case II in Section III is used to find the initial guess trajectory. This initial guess is not shown in Fig. 5 since it does not satisfy the kinematic constraints. The optimal trajectory at different time instants are shown in Fig. 5. Similar to the example in Section IV-A, the five-bar changes output mode twice at $\boldsymbol{p}_1$ and $\boldsymbol{p}_2$ where the links in $\boldsymbol{B}_0\boldsymbol{DF}$ and $\boldsymbol{A}_0\boldsymbol{CP}$ align as shown in Figs. 5(b) and 5(c), respectively. The output mode after crossing $\boldsymbol{p}_2$ has input singularities shown in Fig. 5(c) that need to be crossed to switch to the input mode to which $\boldsymbol{q}_F$ belongs. The five-bar was seen to cross the input singularity by passing through $\boldsymbol{p}_3$ in the output space or touching the input singularity at $\boldsymbol{p}_3$ in the input space when $\boldsymbol{CD}$ and $\boldsymbol{DF}$ links aligned. Finally, after switching input modes, the five-bar reaches $\boldsymbol{q}_F$ as seen in Fig. 5(d).

The electrical energy loss due to Joule heating was 0.117 J, i.e., $0.094\times$ the minimum required work. The error metrics are found to be $r_p = 3.78 \times 10^{-10}$ m, $r_v = 4.36 \times 10^{-10}$ m/s and $e = 3.09 \times 10^{-5}$ which are less than the tolerances stated in Section III-C. The RMS torques for the actuators at $\boldsymbol{A}_0$ and $\boldsymbol{B}_0$ are 0.162 Nm and 0.228 Nm, respectively. The thermal energy loss was maximum for positive disturbances in torques in Section III-C. For this case, the thermal energy loss with time for the optimal trajectory and feedforward PI control with disturbance in torques (see Section III-C) is plotted in Fig. 6. The total thermal energy loss for feedforward PI control until $T_{ss} = 1.875$ s is 0.027 J higher than that for the optimal trajectory.

V. Discussion

As seen in Section IV-A, changing from the configuration in Fig. 1(a) to the one in Fig. 1(b) required switching output modes twice. Each time the output mode switches, the local differential kinematics of the five-bar changes, which is evident from the changing workspace regions in the output and input space shown in Fig. 4. Therefore, the directional velocity and force transmission ratios change as the output mode changes. This was shown in Section IV-A where the final configuration consumed 80% less electrical power than the initial configuration to statically hold the mechanism. In this case, changing output modes by reconfiguring the five-bar from Fig. 1(a) to Fig. 1(b) changed the workspace and introduced a different lower workspace boundary which enabled the five-bar to support high vertical forces with low actuator torque. Furthermore, the workspace area also increased as can be seen in Fig. 4(c). Compared to the initial guess trajectory, the electrical power loss due to Joule heating for the optimal trajectory was significantly lower since the five-bar stays near the output singularity of $\boldsymbol{A}_0\boldsymbol{CP}$ dyad. In the presence of small constant disturbance in actuator torques, the five-bar was able to reach the same final configuration without much change in electrical power loss due to Joule heating. Thus, switching output modes in this case is robust to changes or disturbances in the optimal trajectory.

Similar observations can be made for Example 2 in Section IV-B where the five-bar had to cross an input singularity to access the upper portion of the workspace. The evolution of states locally around the input singularity is solely dictated by the momentum built in the system before reaching the input singularity since the actuators lose control authority at input singularities. In this case, the trajectory satisfied the kinematic constraints and energy conservation equation within the specified tolerances showing that it is feasible both kinematically and dynamically. In the presence of small constant disturbance in actuator torques, the five-bar was able to switch input and output modes and reach the same final configuration. However, the settling time was higher than that in Example 1 due to high overshoot from the desired trajectory resulting from the momentum built in the system to cross the input singularity.

VI. Conclusion

Switching output modes can be useful in realizing different workspaces, velocities, and force production at the end-effector. In this work, the problem of switching output modes for the five-bar mechanism was solved using an optimal control approach that included the dynamics of the mechanism. The optimal control problem was set to minimize

actuator torques and solved using a projection-based direct collocation method [9]. Depending on the input modes that the final and initial configurations belonged to, two methods for finding a good initial guess were presented. Using this method, output mode switching for the five-bar mechanism was demonstrated for two different final configurations. In these examples, the five-bar crossed output and/or input singularities to switch output modes and reach the desired configuration. Furthermore, crossing input singularities required momentum based planning since the actuators lose authority in a direction at these singularities. Considering a dynamic model that included the states of all links (more than the degree-of-freedom of the five-bar) enabled singularity-free computations even at physical input and output singularities. This formulation allowed the optimizer to compute trajectories that switched both input and output modes.

REFERENCES

[1] A. Hernandez, O. Altuzarra, V. Petuya, and E. Macho, "Defining Conditions for Nonsingular Transitions Between Assembly Modes," *IEEE Transactions on Robotics*, vol. 25, no. 6, pp. 1438–1447, Dec. 2009.

[2] J. Hesselbach, M. B. Helm, and S. Soetebier, *Connecting Assembly Modes for Workspace Enlargement*. Dordrecht: Springer Netherlands, 2002, pp. 347–356. [Online]. Available: https://doi.org/10.1007/978-94-017-0657-5_37

[3] C. Budde, M. Helm, P. Last, A. Raatz, and J. Hesselbach, *Configuration Switching for Workspace Enlargement*. Berlin, Heidelberg: Springer Berlin Heidelberg, 2011, pp. 175–189. [Online]. Available: https://doi.org/10.1007/978-3-642-16785-0_11

[4] M. Urizar, V. Petuya, O. Altuzarra, and A. Hernandez, "Computing the configuration space for motion planning between assembly modes," in *Computational Kinematics*, A. Kecskeméthy and A. Müller, Eds. Berlin, Heidelberg: Springer Berlin Heidelberg, 2009, pp. 35–42.

[5] E. Macho, O. Altuzarra, C. Pinto, and A. Hernandez, "Workspaces associated to assembly modes of the 5r planar parallel manipulator," *Robotica*, vol. 26, no. 3, p. 395–403, 2008.

[6] P. B. Edwards, A. Baskar, C. Hills, M. Plecnik, and J. D. Hauenstein, "Output mode switching for parallel five-bar manipulators using a graph-based path planner," in *2023 IEEE International Conference on Robotics and Automation (ICRA)*, 2023, pp. 9735–9741.

[7] F. Bourbonnais, P. Bigras, and I. A. Bonev, "Minimum-time trajectory planning and control of a pick-and-place five-bar parallel robot," *IEEE/ASME Transactions on Mechatronics*, vol. 20, no. 2, pp. 740–749, 2015.

[8] C. Mirz, F. Schöler, J. P. Barreto, and B. Corves, "Optimal control based path planning for parallel kinematic manipulators utilising natural motion," in *2018 IEEE 14th International Conference on Automation Science and Engineering (CASE)*, 2018, pp. 223–228.

[9] R. Bordalba, T. Schoels, L. Ros, J. M. Porta, and M. Diehl, "Direct collocation methods for trajectory optimization in constrained robotic systems," *IEEE Transactions on Robotics*, vol. 39, no. 1, pp. 183–202, 2023.

[10] K. M. Lynch and F. C. Park, *Modern Robotics: Mechanics, Planning, and Control*. Cambridge University Press, 2017.

[11] S. Karneswaran and L. Biegler, "Convergence rates for direct transcription of optimal control problems with final-time equality constraints using collocation at radau points," in *2006 American Control Conference*, 2006, pp. 7 pp.–.

[12] S. Echeandia and P. M. Wensing, "Numerical methods to compute the coriolis matrix and christoffel symbols for rigid-body systems," *Journal of Computational and Nonlinear Dynamics*, vol. 16, no. 9, p. 091004, 2021.

[13] J. A. E. Andersson, J. Gillis, G. Horn, J. B. Rawlings, and M. Diehl, "CasADi – A software framework for nonlinear optimization and optimal control," *Mathematical Programming Computation*, vol. 11, no. 1, pp. 1–36, 2019.

[14] A. Wächter and L. T. Biegler, "On the implementation of an interior-point filter line-search algorithm for large-scale nonlinear programming," *Mathematical Programming*, vol. 106, pp. 25–57, 2006.